Journal of the Serbian Society for Computational Mechanics / Vol. 15 / No. 1, 2021 / pp 24-36
(10.24874/jsscm.2021.15.01.02)

ANALYSIS OF THERMAL ENHANCEMENT IN A BAFFLED RECTANGULAR CHANNEL WITH DIFFERENT FORMS OF OUTLET

Sandip Saha[1*], Apurba Narayan Das[2], Santanu Raut[3]

[1] Department of Mathematics, Madanapalle Institute of Technology and Science, Madanapalle, 517325, Andhra Pradesh, India
e-mail: sandip.tfgss@gmail.com
[2] Department of Mathematics, Alipurduar University, Alipurduar, 736121, West Bengal, India
e-mail: apuraiganj1964@gmail.com
[3] Department of Mathematics, Mathabhanga College, Cooch Behar, 736146, West Bengal, India
e-mail: raut_santanu@yahoo.com
**corresponding author*

Abstract

Analysis of the influence of different forms of channel outlet on the heat exchange hydro-thermal characteristics over a rectangular channel embedded with trapezoidal baffle has been made in this paper. Four different forms of the outlets, viz., (I) an outlet similar to the inlet (case-A), (II) two outlets in the upper and lower parts of the exit section (case-B and case-C) and (III) an outlet of length equal to 45% of the inlet (case-D) have been considered. The impact of the outlets has been investigated from the numerical standpoint using computational fluid dynamic software FLUENT, for a two-dimensional model. The results indicate that the thermal exchange rate substantially increases due to the presence of baffles and depends on the form of the outlet. Moreover, the present investigation shows that the position of the outlet and the mixing of nano-particles in the base fluid plays a significant role in the improvement of thermal exchange.

Keywords: Fluid flow, nanoparticles, various outlet formations, FLUENT, thermal exchange**.**

1. Introduction

Last few decades, there has been a growing interest in studying natural convection as well as forced convection thermal exchange through a rectangular duct with baffles. Various techniques have been adopted for the enhancement of thermal convection in thermal exchangers so far, but the simplest and the most effective way is the introduction of turbulators, popularly named baffles, to interrupt the flow through the formation of vortices or making of three-dimensional blending for increasing the heat exchange in thermal exchangers. Recently, some excellent theoretical, as well as experimental studies, have been done regarding channels embedded with various shaped baffles such as plane, triangular, trapezoidal, cubic, and circular. Variations in temperature gradients and cavity configuration play very important roles in various engineering fields, viz., cross-flow thermal exchangers, design of airfoil cooling, gas turbine, and nuclear

reactor (Valencina et al. 2002; Dutta et al. 1998 a, 1998 b; Dutta et al. 2005; Ozceyhan et al. 2008; Wang et al. 2012; Saha et al. 2020; Saha et al. 2021 a, 2021 b).

On the other hand, some recent studies (Ozceyhan et al. 2008; Wang et al. 2012; Saha et al. 2021 c, 2021 d) on heat exchange suggest that thermal exchange through a baffled channel can be improved sufficiently by blending nanoparticles (metal oxides and carbon materials) in fluid flow. Some earlier studies concluded that nanofluids do not improve thermal characteristics such as heat conductivity and thermal exchange coefficients (Demartini et al. 2004; Nasiruddin et al. 2007; Nanan et al. 2017). After that, several authors (Nasiruddin et al. 2007; Saha 2021; Izadi et al. 2018) performed a set of numerical work on thermal exchange coefficient and pressure drop for distinct forms of the canal.

Tanda (2011) observed the effect of different ratios of pitch and height (i.e., 6.66, 10.0, 13.33 and 20.0) on heat transfer over a rectangular single baffled and double baffled channel. In the case of the single baffled channel, he found that the pitch-to-height ratio = 13.33 was significantly superior, but the case with a value of pitch-to-height ratio lower than 13.33 provided better results than in the case of the channel with two baffles. Bilen et al. (2009) performed some research on heat exchange and studied friction properties of turbulent flow in presence of air in a tube with three distinct corrugations. They reported that the rate of heat exchange increased by 63% for circular corrugation, 58% in the case of trapezoidal corrugation, and 47% in the case of rectangular corrugation as compared to the case of the smooth tube. Kamali et al. (2008) made a machine code to observe the thermal exchange through a square container in presence of circular, triangular, and trapezoidal baffles with a decrease in heights in the direction of the flow. Their findings reported that the trapezoidal baffle provided higher thermal enhancement and pressure drop among all the baffles.

Promvonge et al. (2008) experimentally investigated the heat exchange rate for airflow through a channel with a triangular, wedge, and rectangular-shaped baffles. Their observation indicates that the triangular baffle provides the highest thermal enhancement in comparison to other baffles described in the work. For different values of geometric ratio and height of baffle, Manca et al. (2011) studied heat exchange properties of fluid flow through a rectangular duct with triangular, circular, rectangular, and trapezoidal baffles. They found that the Nusselt number enhances with the increase in baffle height. Peng et al. (2001) studied the thermal-hydraulic properties in presence of a V-shaped baffle in a channel with the variations in the angle of inclination with the horizon. They revealed that the highest level of thermal exchange occurs when the baffle is inclined at an angle of 45^0. Chandra et al. (2003) conducted an interesting study on thermal exchange in a turbulent airflow through a container comprising one or more transverse baffles. They found that the thermal exchange rate in a container with two baffles, placed in opposite positions, increases up to 6% of that of one baffle case.

This article expands on the experimental work of Demartini et al. (2004) and the numerical simulation research of Saha et al. (2020b) and Saha et al. (2020c) (2021). Dermitini et al. (2004) did not account for any variation in the channel's outlets, nor did they address the hydro-thermal processes that prompted us to conduct this study. In the current work, the hydrothermal phenomena over a rectangular channel embedded with two trapezoidal baffles in different positions with opposite directions are studied, which has not been addressed so far. As a result, the findings of this study can be highly useful in selecting appropriate baffle layouts for various engineering groups and sectors involved in hydro-thermal phenomena.

2. Physical geometry

In this paper, four horizontal baffled rectangular channels with different forms of the outlet are considered as depicted in Figs. 1a-1d. The upper wall in each of the cases is assumed to be heated at $300K$ and the rest of the walls are kept as insulated, $\left(\frac{\partial u}{\partial x}=0,\frac{\partial u}{\partial y}=0,\frac{\partial v}{\partial x}=0,\frac{\partial v}{\partial y}=0\right)$, outflow boundary condition along with what has been assumed in the outlet section and based on the Reynolds number, inflow velocity (u_{in}) with $T_{in}=293K$ is prescribed in the inlet section. FLUENT software was used for simulation purposes. In this paper, the analysis of hydrothermal phenomena in a rectangular duct with two baffles mounted at each of the walls is performed.

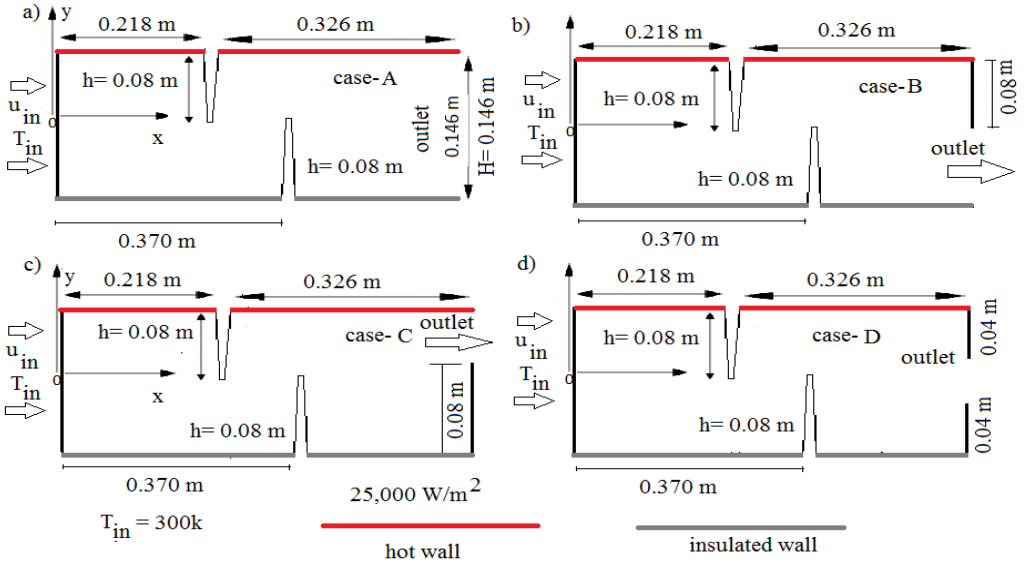

Fig. 1. Rectangular channels with different forms of outlet, (a) type-A, (b) type-B, (c) type-C, (d) type-D.

3. Formulation

The governing equations of this problem (Manca et al. 2011; Manca et al. 2012; Peng 2001; Chandra et al. 2003; Fattah 2012) are as follows:

Equation of continuity:

$$\frac{\partial u}{\partial x}+\frac{\partial v}{\partial y}=0 \tag{1}$$

The momentum of x equation:

$$u\frac{\partial u}{\partial x}+v\frac{\partial u}{\partial y}=-\frac{1}{\rho_{nf}}\frac{\partial p}{\partial x}+\frac{\mu_{nf}}{\rho_{nf}\alpha_{nf}}\frac{1}{\mathrm{Re}}\left(\frac{\partial^2 u}{\partial x^2}+\frac{\partial^2 u}{\partial y^2}\right) \tag{2}$$

The momentum of y equation:

$$u\frac{\partial v}{\partial x}+v\frac{\partial v}{\partial y}=-\frac{1}{\rho_{nf}}\frac{\partial p}{\partial y}+\frac{\mu_{nf}}{\rho_{nf}\alpha_{nf}}\frac{1}{\mathrm{Re}}\left(\frac{\partial^2 v}{\partial x^2}+\frac{\partial^2 v}{\partial y^2}\right) \tag{3}$$

Energy equation:

$$u\frac{\partial T}{\partial x}+v\frac{\partial T}{\partial y}=\frac{\alpha_{nf}}{\alpha_f}\frac{1}{\mathrm{Pr}.\mathrm{Re}}\left(\frac{\partial^2 T}{\partial x^2}+\frac{\partial^2 T}{\partial y^2}\right) \tag{4}$$

Here Re, Nu_{avg} and F denote the Reynolds number, average Nusselt number and friction factor, which are calculated along the lower heated wall and given by (Manca et al. 2011, 2012; Peng 2001; Chandra et al. 2003; Fattah 2012; Gravandyan et al. 2017; Karimipour et al. 2016; Akbari et al. 2016 a, b, c).

$$\mathrm{Re}=\frac{\rho_f H u_{in}}{\mu_f} \tag{5}$$

$$Nu_x=\frac{h_x H}{k_f} \tag{6}$$

$$C_f=\frac{\tau_w}{2\rho_f u_{in}^2} \tag{7}$$

$$\Delta p=\mid p_{out}-p_{in}\mid \tag{8}$$

$$F=\frac{2H\Delta p}{0.554\rho_f u_{in}^2} \tag{9}$$

where $\rho, \mu, h(x), k, p_{out}, nf, f, \gamma, Pr, T, v, u, v$ and $, p_{in}$ are defined as density (kgm^{-3}), dynamic viscosity, coefficient of convective heat transfer, thermal conductivity ($Wm^{-1}K^{-1}$), pressure at outlet, nanofluid, base fluid, thermal diffusivity (m^2s^{-1}), Prandtl number, temperature, kinematic viscosity ($m^2\ s^{-1}$), components of velocity in x, y directions (ms^{-1}), pressure at the inlet, respectively. FVM (Gravandyan et al. 2017; Karimipour et al. 2016; Akbari et al. 2016 a, b, c) are employed to visualize the simulation results. Using a second-order upwind scheme (Gravandyan et al. 2017; Karimipour et al. 2016; Akbari et al. 2016 a, b, c; Zadkhast et al., 2017), the hydrothermal characteristics are studied. In this paper, 10^{-6} is set as convergence criteria (Gravandyan et al., 2017; Karimipour et al., 2016; Akbari et al., 2016 a, b, c).

3.1. Properties of nanofluid

For computing the nanofluid density (ρ_{nf}) and specific nanofluid heat capacity $(\rho C_p)_{nf}$, we used (Gravandyan et al. 2017; Karimipour et al. 2016; Akbari et al. 2016 a, b, c; Yari et al. 2015)

$$\rho_{nf}=(1-D)\rho_f+D\rho_{np} \tag{10}$$

$$(\rho C_p)_{nf}=(1-D)(\rho C_p)_f+D(\rho C_p)_{np} \tag{11}$$

Where ρ_f, ρ_{nf}, $(\rho C_p)_f$, $(\rho C_p)_{np}$ and D denote base fluid and solid nanoparticles mass densities and base fluid, solid nanoparticles heat capacities and volume fraction of nanoparticles. The following means that empirical correlation (Vajjha et al. 2009; Yari et al. 2015) is accomplished to calculate the effective thermal conductivity (k_{ef}) and effective viscosity (μ_{ef}) in the baffle-corrugation channel.

$$k_{ef} = k_{Static} + k_{Brownian} \tag{12}$$

or,

$$k_{ef} = \left[k_f \left[\frac{1 - 2D\frac{(k_f - k_{np})}{(2k_f + k_{np})}}{1 + D\frac{(k_f + k_{np})}{(2k_f + k_{np})}} \right] + 50000 * \alpha * D * \rho_f * C_{pf} \sqrt{\frac{kT}{2\rho_{np} R_{np}}} f(T, D) \right] \tag{13}$$

with

$$f(T, D) = \left[(0.28217D + 0.003917)\frac{T}{T_0} + (-0.030669D - 0.00391123) \right] \tag{14}$$

$$\mu_{ef} = \left[\frac{\mu_f}{1 - 34.87\frac{dp}{d_f} - 0.3D^{1.3}} \right] \tag{15}$$

The value of k is taken as per Vajjha et al. (2010). The value of α of Al_2O_3 is given in Table 1. Table 2 presents thermophysical properties of various base fluids and nanofluid nanoparticles (Lienhard et al. 2006; Corcoine et al. 2009).

material	*α*	*D%*	*T(K)*
Al_2O_3	*$8.44 \times (100\psi)^{-1.07}$*	*[1-10]*	*[298-363]*

Table 1. α of various materials (Vajjha et al. 2009; Yari et al. 2015).

Properties	*Water*	*Al_2O_3*
C_p	*4182*	*765*
ρ	*998.2*	*3970*
k	*0.6*	*40*
μ	*0.001*	—

Table 2. Material characteristics at $T_{in} = 300K$ (Alipour et al. 2016; Zadkhast et al. 2017).

3.2 Numerical procedures

The numerical simulations in this paper are performed by solving the equations [1-4] with the use of boundary conditions. A first-order central difference is used to simulate the diffusion term in momentum and energy equations, which yields a stable solution, and a second-order upwind differencing technique is used for the convective term. To solve the flow field, an iterative approach, namely, SIMPLE algorithm (Gravandyan et al. 2017; Karimipour et al. 2016) is utilized, where the computation is initialized by specifying the pressure field and the velocity components are taken into account to solve the equation of momentum. Due to the absence of pressure term in the equation of continuity, it can easily be transformed into an equation of pressure correction (Gravandyan et al. 2017; Karimipour et al. 2016), and 10^{-6} is set as convergence criteria.

3.3 Grid test and code validation

Grid test (Fig. 2) is done at Re = 87,300 in the presence of two trapezoidal baffles to evaluate the impact of grid sizes on the simulated findings, similar to Demartini et al. (2004) and Saha et al. (2020b). According to Figure 2, 20,000 elements are sufficient to perform the current work (Demartini et al. 2004; Saha et al. 2020b). The code is validated using the same geometrical configuration and boundary circumstances, as Demartini et al. (2004), in which two plane baffles are alternately installed on the channel walls. Figures 3(a-d) show a strong agreement between Demartini et al. (2004) and the current investigation at various locations and at Re = 87300.

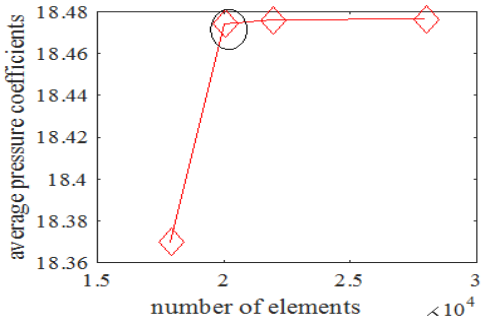

Fig. 2. Average pressure coefficients vs. the total number of elements.

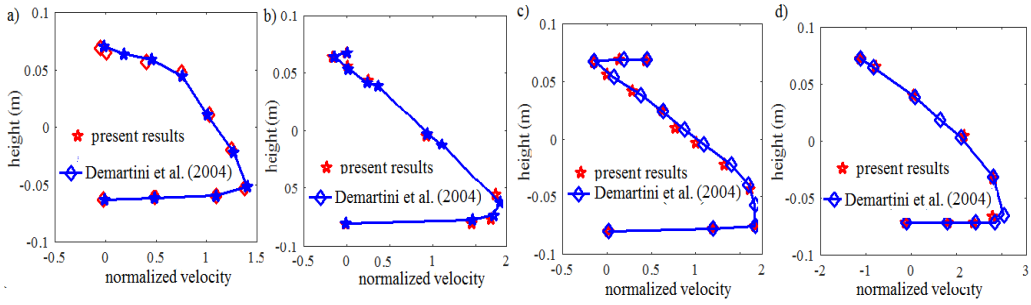

Fig. 3. Profile of normalized velocity at different positions viz., at (a) $x = 0.159\ m$, (b) $x = 0.189m$, (c) $x = 0.289\ m$ and (d) $x = 0.535m$.

4. Analysis of Results

4.1 Velocity magnitude and Dynamic pressure

Figure 4(a-d) represents the profiles of the magnitude of velocity for the different forms of outlets and the profiles of dynamic pressure for various flow fields are described in Figure 4(e-f). Four distinct models with different forms of the outlet are considered as follows:

- the first one is taken as the total flow area between the walls of the rectangular duct (Fig. 4a),
- the second outlet is attached to the upper hot wall of the canal only (Fig. 4b),
- the third outlet is attached to the lower insulated wall of the canal only (Fig. 4c),

- The last one is placed at the middle of the right wall occupying approximately 45% of it (Fig. 4d).

The entire investigation is done for a particular value of the Re. In case (a), the velocity enhances at the top of the first baffle but decreases just after the first baffle due to the decrease in pressure there. Pressure rises in the regions surrounding each baffle as the fluid flow is bifurcated in two streams. Reverse recycling cells are also observed. It is concluded that the flow velocity rises significantly at the top edge of the second baffle. It is to be noted that the pressure rises highly in the region close to the upper wall of the channel after crossing the second baffle. The increase in pressure due to the decrease in flow area is caused by the presence of an obstacle. It is observed that pressure rises to 19.7% in the second form of the outlet and decreases by $24\%, 20.8, \%$ and 18.7% in the first, third and fourth form of the outlets respectively in comparison to the smooth channel.

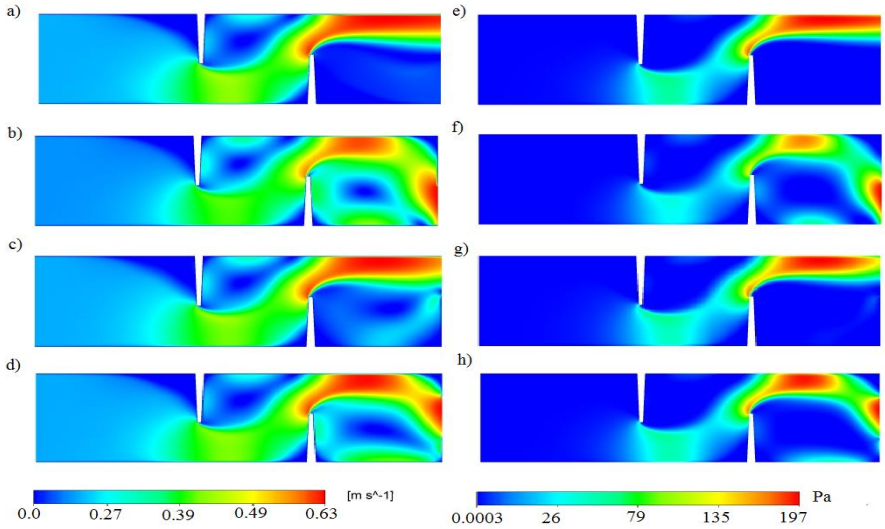

Fig. 4. Profile of (a-d) velocity magnitude and (e-h) dynamic pressure.

4.2 Streamlines

Figure 5 presents the current lines flowing through all the channels considered here. The fluid flow in the canal is disturbed initially by the first baffle fixed on the upper wall. A small recycling zone is found in front of the first baffle and a comparatively larger one is observed at the back side of the first baffle as pressure drops suddenly in that zone. However, the major part of the flow moves towards the top of the second baffle. Finally, the largest part of the fluid exits through the outlet, and a recycling cell is again formed behind the second baffle due to the drop in pressure there caused by that baffle. In the cases of type-A and type-C channels, the fluid exits through the region attached at the upper wall of the channel while the main stream moves towards the middle of the channel in the cases of type-B and type-D channels. At the location x = 0.410 m, flow velocity attains its maximum value which is $4.48, 5.16, 4.57, 4.59$ times of the input reference velocity for type-A, type-B, type-C, and type-D channels, respectively.

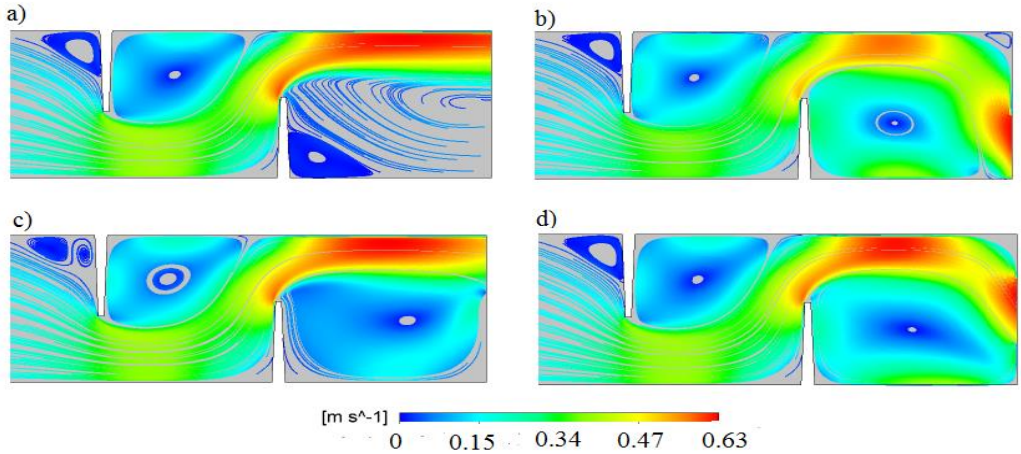

Fig. 5. Streamlines for various formations of an outlet.

4.3 Axial velocity and tangential velocity

Figure 6 (a-d) presents the contours of the axial velocity for various forms of the baffled channel. It is observed that the fluid flows with lower speed after the baffles in all the cases; even negative velocity of the fluid flow appears for which recycling cells formed behind each of the baffles. It is noted that the speed of the fluid flow enhances suddenly in the lower surface of the channel after the first baffle. The main stream is then directed towards the zone located between the upper surface and the top of the second baffle where the axial velocity significantly rises and the flow moves towards the hot upper wall of the channel. In the case of the type-B channel, the maximum axial velocity value reaches up to $0.577\ m/s$, which decreases by $5\%, 3\%$ and 3.3% in cases of type-A, type-D, and type-C channels respectively.

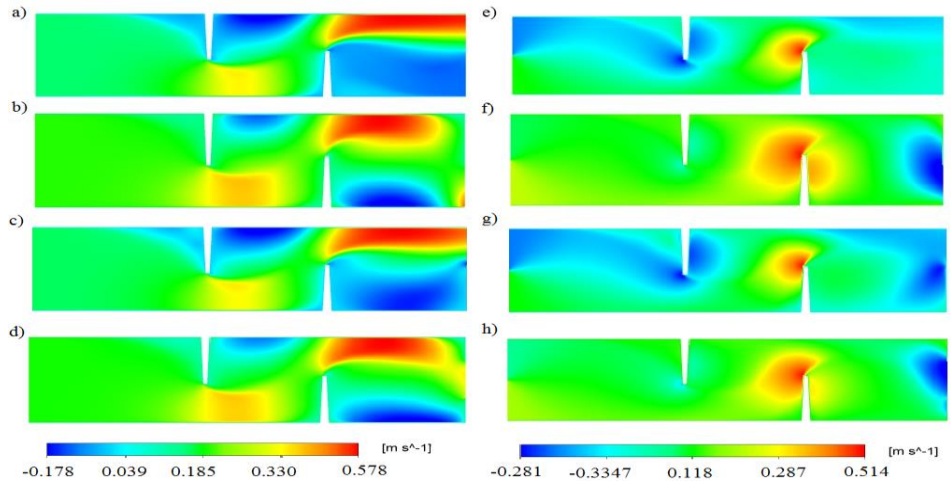

Fig. 6. Profile of (a-d) axial velocity and (e-h) tangential velocity.

The profiles of the transverse velocity are depicted in Fig.6 (e-h), where the fluid velocity substantially decreases in the upper wall of the channel, especially in cases of type-A and type-C channels. The velocity decreases at the tip of the first baffle. It is found that fluid velocity

significantly rises at top of the left side of the second baffle. However, in the cases of type-B and type-D channels, the velocity of the flow is found higher than in the other cases of the outlet. It is observed that the type-B channel has the maximum axial velocity value $0.514\ m/s$, which also decreases by $15\%, 8\%$ and 7.3% in the case of type-A, type-D, and type-C channels respectively.

4.4 Turbulence kinetic energy (TKE) and turbulent intensity (TE)

The kinetic energy is generally found to be very low after the baffle in each of the cases. Fig. 7 (a-d) shows the variations in kinetic energy for various formations of the outlet. The highest value of kinetic energy is attained at the top of the baffle. As compared to the type-B channel, energy drops up to $57\%, 55\%$, and 59% in the cases of type-A, type-C, and type-D channels respectively. The profiles of turbulence intensity for different baffle arrangements in a rectangular channel are depicted in Fig. 7 (e-h). The baffles interrupt the flow and turbulence intensity rises suddenly at the time of contact with the baffle attached to the upper wall. It is interesting to watch how intensity remarkably augments (except in the case of the type-B channel) in the domain adjacent to the top of the second baffle and the upper surface of the channel. In the cases of type-A, type-B, type-C, and type-D channels, turbulence intensities become approximately $13.6\%, 20.8\%, 13.8\%$, and 13.7% respectively, as shown in Fig. 9 in comparison to the smooth channel**.**

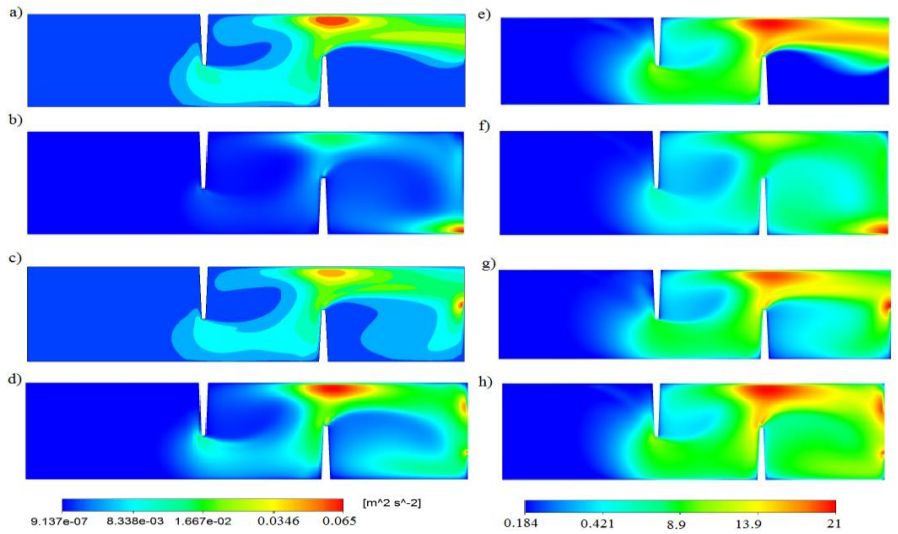

Fig. 7. Profile of (a-d) TKE and (e-h) TE.

4.5 Skin factor, friction coefficient and Nusselt number

Figure 8(a) presents the profiles of Nu_x with the variation in axial positions of different outlet formations. Variations of C_f along the hot walls in distinct models are depicted in Fig. 8 (b). The friction coefficient suddenly drops to almost zero when the flow crosses the baffle. Again, the values of C_f increases partially in recycling zones. After that, it gradually rises in the region next to the second baffle until it attains its highest value there. The rise of skin factors arises due to the deviation of the fluid flow. The friction value finally reduces near the outlet of the channel because of the direct field collision with the hot surface. It is revealed that, for all the cases, the Nusselt number is reduced after the baffle because of the gradual decrease in the contact region of the base fluid with the hot wall of the duct. Again, after the baffle, the value of the Nusselt number rises suddenly due to the rapid increase in the flow in that area. The enhancement in the

heat gradient helps to moderate heat exchange. The thermal exchange rate also enhances in the regions having recycling cells. The heat exchange is improved substantially in the last three cases in comparison to the first case indicating that the thermal exchange rate depends on the position and size of the outlet of the canal. Maximum thermal exchange is found to occur when the outlet is in the center of the canal.

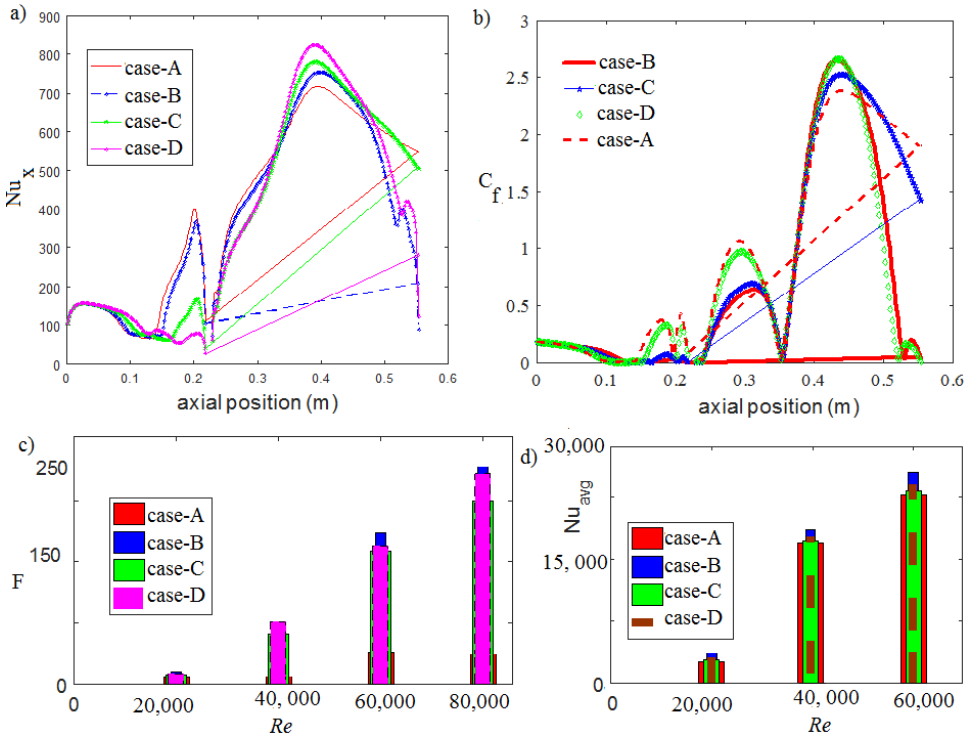

Fig. 8. Variations of (a) Nu_x, (b) C_f, (c) F and (d) Nu_{avg}.

Figure 8(c) describes the variation of the average Nusselt number (Nu_{avg}) against the Re for all the channels. It is clear that Nu_{avg} increases with the increase of Re. The enhancement in Re due to the rise in flow velocity causes disturbance in the flow and also causes the formation of recycling cells in different sections of the channels. In the case of the type-B channel, we can see from Fig. 8(a) that the maximum augmentation in thermal exchange occurs. Figures 8(a) and 8(d) indicate that a quantitative development in the thermal exchange rate arises in all the cases of the baffled channels in comparison to the smooth channel.

5. Conclusions

In this paper, a systematic numerical calculation has been done to study the hydro-thermal phenomena of turbulent fluid flow through a horizontal canal. The lower surface of the canal is kept as insulated whereas the upper surface is kept under constant temperature. In this observation, two baffles are introduced in opposite directions, one is attached at the upper hot wall and another is placed on the lower adiabatic wall. The baffles create turbulence and recycling zones, which enhance heat exchange. Apart from this, the position of the outlet area has a significant effect on heat exchange. The impact of the introduction of baffle and nano-particles

has been investigated from a numerical standpoint using FLUENT software. The consequence and effectiveness of the baffles are ensured from the simulations described in this work. We have concluded that the shape and position of the outlet in a channel play a significant role in modifying the thermal exchange rate in the system.

Acknowledgment - The authors would like to express their gratitude to the reviewer for his helpful recommendations for improving the work.

References

Akbari OA, Karimipour A, Toghraie D, Safaei RM, Alipour GMH, Dahari M (2016 a). Investigation of Rib's height effect on heat transfer and flow parameters of laminar water-Al_2O_3 nanofluid in a two-dimensional rib-microchannel, Appl Math Comp, 290: 135-153.

Akbari OA, Karimipour A, Toghraie D, Karimipour A (2016 b). Impact of ribs on flow parameters and laminar heat transfer of Water-Aluminum oxide nanofluid with different nanoparticle volume fractions in a three-dimensional rectangular microchannel, Adv Mech Eng, 7: 1-11.

Akbari OA, Goodarzi M, Safaei RM, Zarringhalam M, Shabani GAS, Dahari M (2016 c). A modified two-phase mixture model of nanofluid flow and heat transfer in 3-d curved microtube, Adv Powder Tech, 27: 2175-2185.

Alipour H, Karimipour A, Safaei RM, Semiromi DT, Akbari OA (2016). Influence of T-semi attached rib on turbulent flow and heat transfer parameters of a silver–water nanofluid with different volume fractions in a three-dimensional trapezoidal microchannel, Phys E, 88: 60-76.

Bilen K, Cetin M, Gul H, Balta T (2009). The investigation of groove geometry effect on heat transfer for internally grooved tubes, Appl. Therm. Eng, 29 (4): 753-761.

Chandra P, Alexander C, Han J (2003). Heat transfer and friction behaviors in rectangular channels with varying number of ribbed walls, Int. J. Heat Mass Transf. 46 (3): 481-495.

Corcione M (2009). Heat transfer features of buoyancy-driven nanofluids inside rectangular enclosures differentially heated at the sidewalls. International Journal of Thermal Sciences, 49: 1536-1546.

Demartini LC, Vielmo HA, Möller SV (2004). Numeric and experimental analysis of the turbulent flow through a channel with baffle plates, J Braz Soc Mech Sci Eng, 26: 153–159.

Dutta P, Hossain A. (2005). Internal cooling augmentation in rectangular channel using two inclined baffles, International Journal of Heat and Fluid Flow, 26 (2): 223-232.

Dutta P, Dutta S (1998a). Effect of baffle size, perforation, and orientation on internal heat transfer enhancement, Int J Heat Mass Transf, 41: 3005-3013.

Dutta S, Dutta P, Jones RE, Khan JA (1998b). Heat transfer coefficient enhancement with perforated baffles, ASME J Heat Transf, 120: 795-797.

Fattah A (2012). Control of the Separation Flow in a Sudden Enlargement, Journal of Applied Fluid Mechanics, 5 (1): 57-66.

Gravndyan Q, Akbari OA, Toghraie D, Marzban A, Mashayekhi R, Karimi R, Pourfattah F (2017). The effect of aspect ratios of rib on the heat transfer and laminar water/ TiO_2 nanofluid flow in a two-dimensional rectangular microchannel, J Mol Liq, 236: 254-265.

Karimipour A, Alipour H, Akbari OA, Semiromi DT, Esfe MH (2016). Studying the effect of indentation on flow parameters and slow heat transfer of water-silver nano-fluid with varying volume fraction in a rectangular two-dimensional micro channel, Indian J Sci Technol, 8: 2015- 2025.

Kamali R, Binesh RA (2008). The importance of rib shape effects on the local heat transfer and flow friction characteristics of square ducts with ribbed internal surfaces, Int. Commun. Heat Mass Transf, 35 (8): 1032-1040.

Izadi M, Pour SMRH, Yasuri AK, Chamkha AJ (2018). Mixed convection of a nanouid in a three-dimensional channel: Effect of opposed buoyancy force on hydro-dynamic parameters, thermal parameters and entropy generation, Journal of Thermal Analysis and Calorimetry, 136 (6): 2461-2475.

Lienhard VI, Lienhard V (2006). A Heat Transfer Textbook, Third Edition Phlogiston Press.

Manca O, Nardini S, Ricci D (2011). Numerical analysis of water forced convection in channels with differently shaped transverse ribs, J. Appl. Math, 2011: 23-37.

Manca O, Nardini S, Ricci D (2012). A numerical study of nanofluid forced convection in ribbed channels, Appl. Therm. Eng, 37: 280-292.

Nanan K, Thianpong C, Pimsarn M, Chuwattanakul V, Eiamsaard S (2017). Flow and thermal mechanisms in a heat exchanger tube inserted with twisted cross-baffle turbulators, Applied Thermal Engineering, 114: 130-147.

Nassiruddin MH, Siddiqui K (2007). Heat transfer augmentation in a heat exchanger tube using a baffle, International Journal of Heat and Fluid Flow, 28 (2): 318-328.

Ozceyhan V, Gunes S, Buyukalaca O, Altuntop N. (2008). Heat transfer enhancement in a tube using circular cross-sectional rings separated from wall, Applied Energy, 85 (10): 988-1001.

Peng W, Jiang XP, Wang PY, Wei YB (2011). Experimental and numerical investigation of convection heat transfer in channels with different ribs, Appl. Therm. Eng, 31(14-15): 2702-2708.

Promvonge P, Thianpong C (2008). Thermal performance assessment of turbulent channel flows over different shaped ribs, Int. Commun. Heat Mass Transfer, 35 (10), 1327-1334.

Saha S, Biswas P, Nath S (2020a). Bifurcation phenomena for incompressible laminar flow in expansion channel to study Coanda effect**,** Journal of Interdisciplinary Mathematics, 23 (2): 493-502.

Saha S, Biswas P, Nath S, Singh L (2020b). Numerical simulations of Newtonian fluid flow through a suddenly contracted rectangular channel with two different types of baffle plates, Soft Computing, 25: 9873-9885.

Saha S (2021). Numerical simulation of turbulent airflow and heat transfer through a rectangular channel along with two trapezoidal baffle plates: comparison between plane and trapezoidal shape baffles plates, AIP Conference Proceedings, 2341 (040035), 1-10.

Saha S, Biswas P, Raut S, Das NA (2021a). Convective heat transfer of laminar nano-fluids flow through a rectangular micro-channel with different types of baffle-corrugation**,** International Journal for Computational Methods in Engineering Science & Mechanics, 22 (2): doi.org/10.1080/15502287.2021.1894509**.**

Saha S, Raut S, Das NA (2021b). Thermal enhancement and entropy generation of laminar water-Al_2O_3 nano-fluid flow through a sudden expansion channel with bell-shaped surface, International Journal of Fluid Mechanic Research, 48 (3): 65-78.

Saha S, Biswas P, Raut S, Das NA (2021c). Analysis of heat transfer characteristics through a rectangular enclosure, Materials today proceedings, 47 (11): 2905-2911.

Saha S, Raut S, Das NA (2021d). Numerical simulations of heat transfer phenomena through a baffled rectangular channel, International Journal of Mathematical, Engineering and Management Sciences, 6 (5): 1230-1241.

Tanda G. (2011). Effect of rib spacing on heat transfer and friction in a rectangular channel with 45° angled rib turbulators on one/two walls, Int. J. Heat Mass Transf, 54 (5): 1081-1090.

Vajjha SR, Das DK (2009). Experimental determination of thermal conductivity of three nanofluids and development of new correlations, International Journal of Heat and Mass Transfer, 52: 4675- 4682.

Vajjha SR, Das DK (2010). Development of new correlations for convective heat transfer and friction factor in turbulent regime for nanofluids, International Journal of Heat and Mass Transfer, 53: 4607-4618.

Valencia A, Cid M (2002). Turbulent unsteady flow and heat transfer in channels with periodically mounted square bars, International Journal of Heat and Mass Transfer, 45 (8): 1661-1673.

Wang F, Zhang J, Wang S (2012). Investigation on flow and heat transfer characteristics in rectangular channel with drop-shaped pin fins, Propulsion and Power Research, 1 (1): 64-70.

Yari G Z, Haghshenasfard M, Nasr EM (2015). Investigation of nanofluids heat transfer in a ribbed microchannel heat sink using single-phase and multiphase CFD models, Int Commun Heat Mass Transf, 68: 122-129.

Zadkhast M, Toghraie D, Karimipour A (2017). Developing a new correlation to estimate the thermal conductivity of MWCNT CuO/water hybrid nanofluid via an experimental investigation, J Therm Anal Calorim, 129: 859-867.